

Article

First-Principles Forecast of Gapless Half-Metallic and Spin-Gapless Semiconducting Materials: Case Study of Inverse Ti_2CoSi -Based Compounds

Liang Zhang ¹, Shengjie Dong ^{2,*}, Jiangtao Du ¹, Yi-Lin Lu ³, Hui Zhao ⁴ and Liefeng Feng ^{1,*} 

¹ Tianjin Key Laboratory of Low Dimensional Materials Physics and Preparing Technology, Department of Physics, Faculty of Science, Tianjin University, Tianjin 300350, China; liang_zhang@tju.edu.cn (L.Z.); 2014210001@tju.edu.cn (J.D.)

² Faculty of Education and Sports, Guangdong Baiyun University, Guangzhou 510450, China

³ College of New Energy, Bohai University, Jinzhou 121007, China; yilinlu@tju.edu.cn

⁴ Department of Physics, College of Physics and Materials Science, Tianjin Normal University, Tianjin 300387, China; naihuizhao@gmail.com

* Correspondence: shengjiedong@tju.edu.cn (S.D.); fengliefeng@tju.edu.cn (L.F.); Tel.: +86-1862-273-0034 (L.F.)

Received: 23 December 2019; Accepted: 20 January 2020; Published: 22 January 2020



Featured Application: Half of the Si atoms in $\text{Ti}_{2.25}\text{Co}_{0.75}\text{Si}$ are replaced by B, Al, Ga, P, As, and Sb, and the results show that doped Ti_2CoSi with an appropriate concentration of impurities could exhibit half-metallic ferromagnetic, gapless half-metallic, and spin-gapless semiconducting states.

Abstract: First-principles calculations were used to investigate several inverse Ti_2CoSi -based compounds. Our results indicate that Ti_2CoSi could transform from a spin-gapless semiconductor to a half metal if a quarter of the Co atoms are replaced by Ti. $\text{Ti}_{2.25}\text{Co}_{0.75}\text{Si}$ would keep stable half-metallic properties in a large range of lattice parameter under the effect of hydrostatic strain, and would become a gapless half metal under the effect of tetragonal distortion. Furthermore, we substituted B, Al, Ga, P, As, and Sb for Si in the $\text{Ti}_{2.25}\text{Co}_{0.75}\text{Si}$ compound. Our results demonstrate that $\text{Ti}_{2.25}\text{Co}_{0.75}\text{Si}_{0.5}\text{B}_{0.5}$, $\text{Ti}_{2.25}\text{Co}_{0.75}\text{Si}_{0.5}\text{Al}_{0.5}$, and $\text{Ti}_{2.25}\text{Co}_{0.75}\text{Si}_{0.5}\text{Ga}_{0.5}$ are half-metallic ferromagnetic materials, and $\text{Ti}_{2.25}\text{Co}_{0.75}\text{Si}_{0.5}\text{P}_{0.5}$, $\text{Ti}_{2.25}\text{Co}_{0.75}\text{Si}_{0.5}\text{As}_{0.5}$, and $\text{Ti}_{2.25}\text{Co}_{0.75}\text{Si}_{0.5}\text{Sb}_{0.5}$ are spin-gapless semiconducting materials. The introduced impurity atoms may adjust the valence electron configuration, change the charge concentration, and shift the location of the Fermi level.

Keywords: first-principles calculation; Heusler compounds; gapless half metals; spin gapless semiconductor

1. Introduction

With the development of nanotechnology and computational materials science, spintronics has developed rapidly in the past 30 years. In order to improve the performance of spin diodes, spin valves, and spin filters, the design of high spin-polarized materials has attracted much attention [1–4]. For half-metallic ferromagnetic compounds with unique electronic structures, one of the two spin channels is semiconducting and the other is metallic. As promising spintronic candidates, they exhibit a complete spin polarization of carriers near the Fermi level [5–12]. A spin-gapless semiconductor is another new kind of spintronic material, which has an almost complete spin polarization and good compatibility with the existing semiconductor industry. By shifting the Fermi energy at the finite gate voltage, the spin-polarized transport properties of spin-gapless semiconductors can be tuned, which has great prospects for future spintronic applications [13,14].

Half metals and spin-gapless semiconductors are special kinds of materials. Because of their unique electronic structures, they have novel spin-dependent electronic properties. The band structure of these materials has only one energy gap for a specific spin direction, which means that the band gap disappears in the opposite spin direction. This phenomenon leads to the application prospects of high carrier spin polarization and spin-controlled electrical and magnetic features. In recent years, in order to develop new technologies involving spintronics, it has been important to search for new materials with these characteristics. Many of these materials are Heusler alloys with a specific crystalline ordering, which is very important for the unique electronic and magnetic properties of these materials. Therefore, it is crucial to study these alloys and compounds with these novel physical properties.

Heusler alloys are named for the German mining engineer and chemist Friedrich Heusler, who investigated Cu–Mn–Al alloys around the year 1900. Heusler compounds are ternary intermetallic compounds, which have been known since 1903 [15]. These alloys were interesting because some of them were ferromagnetic, even though their constituent atoms were non-ferromagnetic as elements. At that time, Cu_2MnAl compounds were proven to be ferromagnetic, although none of the three elements were ferromagnetic. The structure of the alloys was later found to be face-centered cubic (fcc) with a four-atom basis consisting of a single formula unit. Thus, members of this Heusler family with a formula unit A_2BC (known as “full” Heuslers) can be viewed as layers consisting of a square lattice of “A” atoms alternating with layers of “B” and “C” atoms, as shown in Figure 1a. A related Heusler family has members with the formula unit ABC, in which half of the “A” atoms of the full Heusler are replaced by vacancies, as shown in Figure 1b. These are known as “half” Heuslers or semi-Heuslers. A third Heusler family with the formula unit A_2BC (similar to the “full” Heuslers) consists of alloys that can be viewed as “AB” layers alternating with “AC” layers, as shown in Figure 1c. These are known as “inverse” Heuslers.

The properties of Heusler compounds can be altered by element substitution, but no single set of properties can characterize the entire Heusler family. Heusler alloys are expected to play an important role in spintronics, magneto-optical reading–recording devices, magnetic tunnel junctions, or tunneling magnetoresistance devices, due to their various multifunctional magnetic properties [16,17]. In the past years, several inverse binary- and ternary-Heusler alloys with a high Curie temperature, as well as quaternary-Heusler alloys, were theoretically predicated to exhibit spin-gapless semiconducting electronic structures [18,19]. Moreover, the bulk and thin films of Mn_2CoAl and Ti_2MnAl films were experimentally fabricated [20–23]. More recently, with first principle calculations, $\text{Ti}_2\text{MnAl}_{0.5}\text{Sn}_{0.5}$ and $\text{Ti}_2\text{MnAl}_{0.5}\text{In}_{0.5}$ were proven to be half metal and spin-gapless semiconductor, respectively [24].

Magnetic Heusler compounds are widely used in spintronic applications. The Heusler semiconductor can be used as either a spin-conserved tunneling barrier or a spin-transporting spacer in a Heusler ferromagnet–Heusler semiconductor–Heusler ferromagnet heterojunction, which has been extensively investigated in recent years. The magnetic Heusler compound is useful and meaningful for its potential integration into magnetic multilayer devices toward some spin valves, as well as for other opportunities and new phenomena.

In addition to these spintronic applications mentioned above, Heusler compounds, with other excellent properties, were studied extensively in the past several years. For instance, several Heusler compounds can be used as solar cell materials, thermoelectric materials, topological materials, magneto-optical materials, magneto-caloric materials, shape-memory materials, heavy-Fermion materials, superconductors, semiconductors, and so on [25–28].

In this work, the electronic structures and magnetic properties of the Ti_2CoSi inverse Heusler alloy were calculated when a quarter of Co atoms were replaced by Ti. Then, the effects of hydrostatic strain and tetragonal deformation on the electronic structures and magnetic properties of the $\text{Ti}_{2.25}\text{Co}_{0.75}\text{Si}$ compound were studied. Meanwhile, half of the Si atoms in $\text{Ti}_{2.25}\text{Co}_{0.75}\text{Si}$ were replaced by B, Al, Ga, P, As, and Sb, and the results show that doped Ti_2CoSi with an appropriate concentration of impurities could be a half-metallic ferromagnet, a gapless half metal, or a spin-gapless semiconductor.

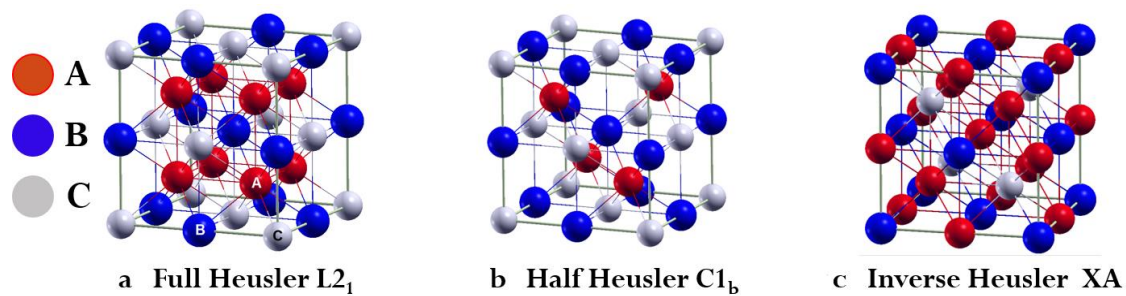


Figure 1. Crystal cell of (a) a full Heusler structure, (b) half Heusler structure, and (c) inverse Heusler structure.

2. Materials and Methods

2.1. Structure of Materials

Structurally, the large Heusler family is described by only two variants, namely: the so-called full-Heusler X_2YZ phase, which is usually crystallized in the Cu_2MnAl -type ($L2_1$) structure, and the half-Heusler XYZ phase with a $C1_b$ structure, where X is a transition metal, Y may be a transition metal or a rare metal, and Z is a main group element. For full-Heusler alloys, if the atomic number of Y is higher than that of X , making the Y element more electronegative than the X element, the inverse Heusler structure of Hg_2CuTi -type can be observed [29]. This structure adopts an $F-43m$ space group, and the atoms obey the following filling rules: X in $(0, 0, 0)$ and $(0.25, 0.25, 0.25)$, and Y and Z in $(0.5, 0.5, 0.5)$ and $(0.75, 0.75, 0.75)$, respectively [30].

2.2. Computational Methods

For investigating the electronic structures and magnetic properties of these pure and doped inverse Heusler alloys, *ab initio* calculations were carried out by using the density functional theory (DFT) with the standard generalized gradient approximations (GGA) of Perdew, Burke, and Erzerhof (PBE) to deal with the exchange correlation functional [31–36]. The cutoff energy for the plane wave was set to be 500 eV, and the k point meshes for the Brillouin zone were set to be $12 \times 12 \times 12$. In addition, the convergence for the difference on the total energy was set to be 1×10^{-6} eV/atom [37,38].

3. Results and Discussion

3.1. Crystal Structures and Lattice Parameters

As shown in Figure 2a, the crystal structure of the regular Heusler alloy Ti_2CoSi has a face-centered cubic structure with the following atomic positions: Ti $(0, 0, 0)$, Ti $(0.5, 0.5, 0.5)$, Co $(0.25, 0.25, 0.25)$, and Si $(0.75, 0.75, 0.75)$. Figure 2b shows that the inverse structure possesses 16 atoms in the unit cell with the following atomic positions: Ti $(0, 0, 0)$, Co $(0.5, 0.5, 0.5)$, Ti $(0.25, 0.25, 0.25)$, and Si $(0.75, 0.75, 0.75)$. From the previous study, it is known that the inverse Heusler alloy Ti_2CoSi is a spin-gapless semiconductor with an integer magnetic moment of $3 \mu_B$ at the equilibrium lattice constant of 6.03 \AA . With the GGA calculations, we found that the inverse Ti_2CoSi alloy evinces gapless semiconducting characteristics at the equilibrium lattice parameter of 6.02 \AA , which derives 0.16% less than from the previous investigation, demonstrating that our research is reasonable.

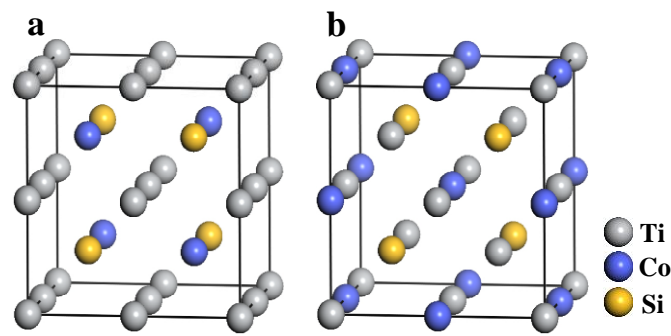


Figure 2. Crystal cell of Ti_2CoSi with (a) regular cubic Heusler structure and (b) an inverse cubic Heusler structure.

For determining the magnetic ground state of these materials, we calculated the energies of the ferromagnetic (FM) and anti-ferromagnetic (AFM) states. The energy differences between the AFM and FM states are listed in Table 1. The positive values illustrate that the energy of the FM state is smaller than that of the AFM state, indicating that the FM state is the magnetic ground state of these materials. At the same time, the minimized energies were obtained by computing the total energy among a large range of lattice parameters. The equilibrium lattice parameters are 6.01 Å and 6.04 Å for $\text{Ti}_{2.25}\text{Co}_{0.75}\text{Si}_{0.5}\text{B}_{0.5}$ and $\text{Ti}_{2.25}\text{Co}_{0.75}\text{Si}_{0.5}\text{P}_{0.5}$, which is smaller than that of $\text{Ti}_{2.25}\text{Co}_{0.75}\text{Si}$, as the radius of Si is larger than that of the B and P atoms. The calculated values are 6.13 Å, 6.13 Å, 6.12 Å, and 6.25 Å for $\text{Ti}_{2.25}\text{Co}_{0.75}\text{Si}_{0.5}\text{Al}_{0.5}$, $\text{Ti}_{2.25}\text{Co}_{0.75}\text{Si}_{0.5}\text{Ga}_{0.5}$, $\text{Ti}_{2.25}\text{Co}_{0.75}\text{Si}_{0.5}\text{As}_{0.5}$, and $\text{Ti}_{2.25}\text{Co}_{0.75}\text{Si}_{0.5}\text{Sb}_{0.5}$, respectively.

3.2. Electronic Structures and Magnetic Properties

The electronic band structures of the $\text{Ti}_{2.25}\text{Co}_{0.75}\text{Si}$ alloy at its equilibrium lattice constant were calculated and are shown in Figure 3a. The spin-up and spin-down electronic bands are indicated by blue and red lines, respectively. When we replaced 25% cobalt with titanium in a cubic cell, a $\text{Ti}_{2.25}\text{Co}_{0.75}\text{Si}$ alloy was achieved. It can be seen that the spin-up direction shows a metallic behavior and the spin-down direction evinces a semiconducting behavior with an indirect band gap of 0.22 eV around the Fermi level. The valence band maximum (VBM) and conduction band minimum (CBM) are located at R and M points, respectively. Thus, $\text{Ti}_{2.25}\text{Co}_{0.75}\text{Si}$ is a half-metallic ferromagnetic material with an integer magnetic moment of 7 μ_B (see Table 1). The calculated values of P were 98% for $\text{Ti}_{2.25}\text{Co}_{0.75}\text{Si}_{0.5}\text{B}_{0.5}$ and $\text{Ti}_{2.25}\text{Co}_{0.75}\text{Si}_{0.5}\text{Ga}_{0.5}$, and 96% for $\text{Ti}_{2.25}\text{Co}_{0.75}\text{Si}_{0.5}\text{P}_{0.5}$, and 100% for the other studied compounds in this work, where $P = [N_{\uparrow}(E_F) - N_{\downarrow}(E_F)] / [N_{\uparrow}(E_F) + N_{\downarrow}(E_F)]$, and $N_{\uparrow,\downarrow}(E_F)$ are the spin-dependent density of states at the Fermi level [39–41].

It is also important to study the effect of the possible lattice distortion during the process of film deposition on the electronic structures. The influences of compression and tetragonalization on the magnetic properties of the $\text{Ti}_{2.25}\text{Co}_{0.75}\text{Si}$ compound were investigated. Figure 4a presents the position of the CBM and VBM of the spin-down channel as a function of the lattice constant. Upon compressing the lattice strain, the half-metallic properties can be kept between a range from 5.78 Å to 6.35 Å, indicating that the half-metallic characteristics of $\text{Ti}_{2.25}\text{Co}_{0.75}\text{Si}$ can be preserved when the lattice constants are changed by -4.9% – 4.4% in relation to the equilibrium lattice constant. Figure 4b presents the position of the CBM and VBM of the spin-down channel as a function of the c/a ratio. Under the influence of tetragonalization, we found that the alloy experiences the transformation from a magnetic metal to a traditional half metal to a gapless half metal, and finally to a magnetic metal. For a $\text{Ti}_{2.25}\text{Co}_{0.75}\text{Si}$ compound, a gapless half metal can be obtained when the lattice parameter, c , is expanded by 12%. The corresponding electronic band structures ($c/a = 1.12$) are plotted in Figure 3b. It can be seen that majority-spin electrons pass through the Fermi level, while the CBM and VBM of the minority spin just touch the Fermi level at R and A points, respectively.

Table 1. The optimized equilibrium lattice parameter, a_0 (Å); the energy difference ΔE (eV) between anti-ferromagnetic (AFM) and ferromagnetic (FM) states; and the total magnetic moment μ_{tot} (μ_B) of the studied compounds.

Compound	a_0	ΔE	μ_{tot}
Ti _{2.25} Co _{0.75} Si	6.08	1.171	7.00
Ti _{2.25} Co _{0.75} Si _{0.5} B _{0.5}	6.01	0.607	5.00
Ti _{2.25} Co _{0.75} Si _{0.5} Al _{0.5}	6.13	0.592	5.00
Ti _{2.25} Co _{0.75} Si _{0.5} Ga _{0.5}	6.13	0.673	5.00
Ti _{2.25} Co _{0.75} Si _{0.5} P _{0.5}	6.04	0.705	8.91
Ti _{2.25} Co _{0.75} Si _{0.5} As _{0.5}	6.12	0.830	9.00
Ti _{2.25} Co _{0.75} Si _{0.5} Sb _{0.5}	6.25	0.963	9.00

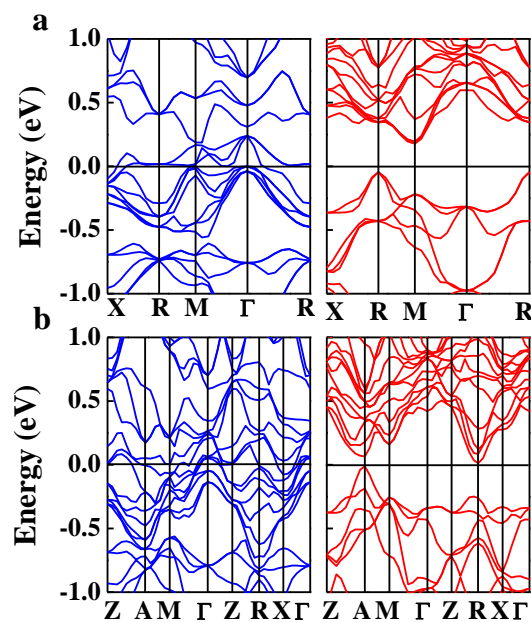


Figure 3. Spin-resolved electronic band structures of Ti_{2.25}Co_{0.75}Si (a) at an equilibrium lattice constant and (b) with $c/a = 1.12$ lattice distortion. The zero of the energy scale is set at the Fermi energy. The blue and red solid lines represent spin-up and spin-down states, respectively.

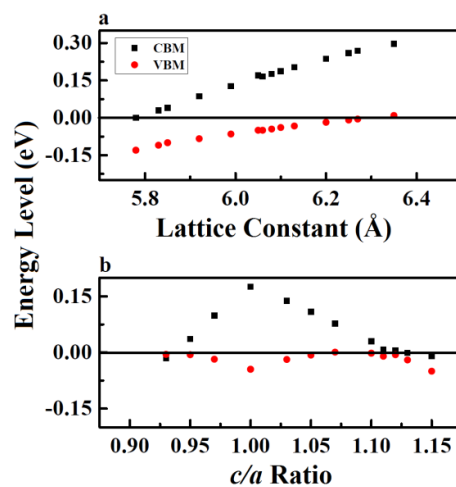


Figure 4. The energy of conduction band minimum (CBM) and valence band maximum (VBM) of the spin-down channel as a function of (a) the lattice constant and (b) the c/a ratio for Ti_{2.25}Co_{0.75}Si.

In the following, we substituted half of the silicon with B, Al, Ga, P, As, and Sb atoms in the cubic cell of $\text{Ti}_{2.25}\text{Co}_{0.75}\text{Si}$ compound. The spin-resolved electronic band structures of the investigated compounds in the equilibrium lattice parameters were computed and are presented in Figures 5 and 6. For $\text{Ti}_{2.25}\text{Co}_{0.75}\text{Si}_{0.5}\text{B}_{0.5}$, $\text{Ti}_{2.25}\text{Co}_{0.75}\text{Si}_{0.5}\text{Al}_{0.5}$, and $\text{Ti}_{2.25}\text{Co}_{0.75}\text{Si}_{0.5}\text{Ga}_{0.5}$, although the Fermi level shifts into a low region of energy with the decrease of the valence electrons, the majority-spin electrons still pass through the Fermi level and the minority-spin bands evince semiconducting characteristics with a band gap, indicating that they are also half metallic. In particular, we found that for $\text{Ti}_{2.25}\text{Co}_{0.75}\text{Si}_{0.5}\text{B}_{0.5}$ and $\text{Ti}_{2.25}\text{Co}_{0.75}\text{Si}_{0.5}\text{Ga}_{0.5}$, the VBM of the spin-down channel touched the Fermi level at T point, demonstrating two quasi-gapless half metals. We also found that the minority spin band gap of $\text{Ti}_{2.25}\text{Co}_{0.75}\text{Si}_{0.5}\text{B}_{0.5}$ was smaller than that of $\text{Ti}_{2.25}\text{Co}_{0.75}\text{Si}_{0.5}\text{Al}_{0.5}$ and $\text{Ti}_{2.25}\text{Co}_{0.75}\text{Si}_{0.5}\text{Ga}_{0.5}$. The reason for this may be that the atomic radius of the boron atom is relatively small, which leads to a certain chemical pressure, and then reduces the band gap. For the cases of $\text{Ti}_{2.25}\text{Co}_{0.75}\text{Si}_{0.5}\text{P}_{0.5}$, $\text{Ti}_{2.25}\text{Co}_{0.75}\text{Si}_{0.5}\text{As}_{0.5}$, and $\text{Ti}_{2.25}\text{Co}_{0.75}\text{Si}_{0.5}\text{Sb}_{0.5}$, the spin-up bands open a seamless gap, and the Fermi level is located at this zero-gap as a result of the increase of valence electrons. Generally speaking, spin-gapless semiconductors can be divided into four categories, as follows: (i) one spin channel is semiconducting and the other spin channel is gapless; (ii) one spin channel is semiconducting and the VBM touches the Fermi level, while the other spin channel is gapless; (iii) there is a gap for both spin-up and spin-down channels, nonetheless, both the VBM of the spin-up channel and the CBM of the spin-down channel are in contact with the Fermi level; and (iv) one spin channel is gapless, and for the other spin channel, the Fermi level touches the edge of the conduction bands. For $\text{Ti}_{2.25}\text{Co}_{0.75}\text{Si}_{0.5}\text{P}_{0.5}$, the spin-up channel is gapless and the CBM touches the Fermi level in the spin-down channel. Thus, it belongs to the fourth type. For $\text{Ti}_{2.25}\text{Co}_{0.75}\text{Si}_{0.5}\text{As}_{0.5}$ and $\text{Ti}_{2.25}\text{Co}_{0.75}\text{Si}_{0.5}\text{Sb}_{0.5}$, the spin-up channel is gapless, while the spin-down channel is semiconducting. As a consequence, they should belong to the first type. Nevertheless, for $\text{Ti}_{2.25}\text{Co}_{0.75}\text{Si}_{0.5}\text{As}_{0.5}$, the CBM of the down spins stand too close to the Fermi level. Thus, the singular electromagnetic transport effect can only be observed at very low temperatures. For $\text{Ti}_{2.25}\text{Co}_{0.75}\text{Si}_{0.5}\text{Sb}_{0.5}$, there is also a very small gap in the spin-up channel. Thereby, strictly speaking, it would be a spin-polarized narrow band-gap semiconductor. However, at a finite temperature, the compound would present the typical electromagnetic transport phenomenon of the spin-gapless semiconductor.

Taking $\text{Ti}_{2.25}\text{Co}_{0.75}\text{Si}_{0.5}\text{B}_{0.5}$ and $\text{Ti}_{2.25}\text{Co}_{0.75}\text{Si}_{0.5}\text{P}_{0.5}$, for example, we discussed the orbital-resolved spin polarization. The total density of the states (DOS) and partial DOS for $\text{Ti}_{2.25}\text{Co}_{0.75}\text{Si}_{0.5}\text{B}_{0.5}$ and $\text{Ti}_{2.25}\text{Co}_{0.75}\text{Si}_{0.5}\text{P}_{0.5}$ obtained using GGA, are presented in Figure 7. The DOS around the Fermi level is heavily dominated by the 3d states of the Ti and Co atoms. It was found that the 3d states of Co are mainly distributed from -1 to -3 eV, while the 3d states of Ti are mainly distributed around and beyond the Fermi level. The electronic configurations of the Ti and Co atoms are $3d^24s^2$ and $3d^74s^2$, respectively. Thus, the Ti atom with less than half of the filling valence electron shell is mainly distributed at high energy levels, and the Co atom with more than half the filling valence electron shell is mainly distributed at low energy levels. It was also found that the impurity atoms play a key role in adjusting the valence electron concentration of the compound, and shift the Fermi level upwards or downwards. For $\text{Ti}_{2.25}\text{Co}_{0.75}\text{Si}_{0.5}\text{B}_{0.5}$, the acceptor doping moves the Fermi level downwards, and thus the Fermi level is submerged in the deeper energy region. For $\text{Ti}_{2.25}\text{Co}_{0.75}\text{Si}_{0.5}\text{P}_{0.5}$, the donor doping moves the Fermi level upwards, and thus the Fermi level is able to be pulled out of the filled bands and is located at the nearly zero band gap.

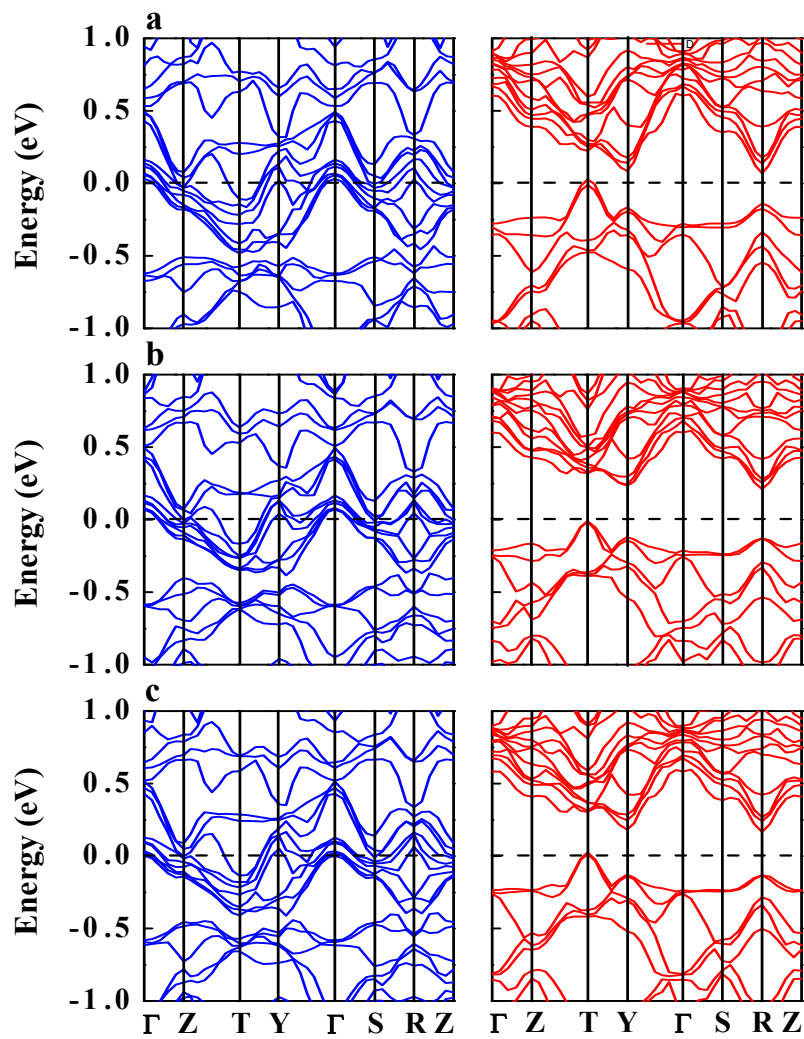


Figure 5. Spin-resolved electronic band structures of (a) $\text{Ti}_{2.25}\text{Co}_{0.75}\text{Si}_{0.5}\text{B}_{0.5}$, (b) $\text{Ti}_{2.25}\text{Co}_{0.75}\text{Si}_{0.5}\text{Al}_{0.5}$, and (c) $\text{Ti}_{2.25}\text{Co}_{0.75}\text{Si}_{0.5}\text{Ga}_{0.5}$ at the equilibrium lattice parameters. The zero of the energy scale is set at the Fermi energy. The blue and red solid lines represent the spin-up and spin-down states, respectively.

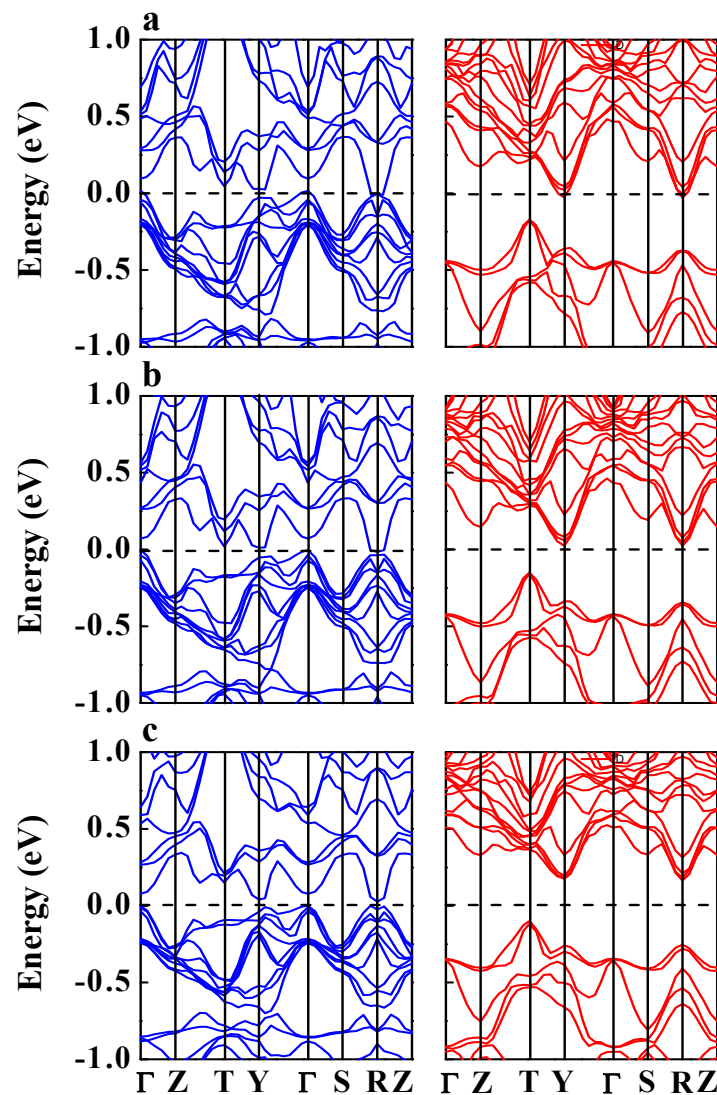


Figure 6. Spin-resolved electronic band structures of (a) $\text{Ti}_{2.25}\text{Co}_{0.75}\text{Si}_{0.5}\text{P}_{0.5}$, (b) $\text{Ti}_{2.25}\text{Co}_{0.75}\text{Si}_{0.5}\text{As}_{0.5}$, (c) and $\text{Ti}_{2.25}\text{Co}_{0.75}\text{Si}_{0.5}\text{Sb}_{0.5}$ at the equilibrium lattice parameters. The zero of the energy scale is set at the Fermi energy. The blue and red solid lines represent the spin-up and spin-down states, respectively.

The results show that the spin-up and spin-down states around the Fermi level are predominantly derived from the Ti-d and Co-d states, and the d–d hybridization is the main origin for spin polarization. In order to understand this matter intuitively, we drew the spin density plots of $\text{Ti}_{2.25}\text{Co}_{0.75}\text{Si}_{0.5}\text{B}_{0.5}$ and $\text{Ti}_{2.25}\text{Co}_{0.75}\text{Si}_{0.5}\text{P}_{0.5}$ (see Figure 8), which are defined as the difference of spin-up and spin-down states. We can see that the spin density predominantly concentrates on the Ti and Co atoms, evincing that the spin polarization is mainly from the Ti and Co atoms. For these compounds, the magnetic moments are predominantly due to the Ti-d and Co-d electrons. The large exchange splitting of the Ti-d and Co-d states leads to a large magnetic moment.

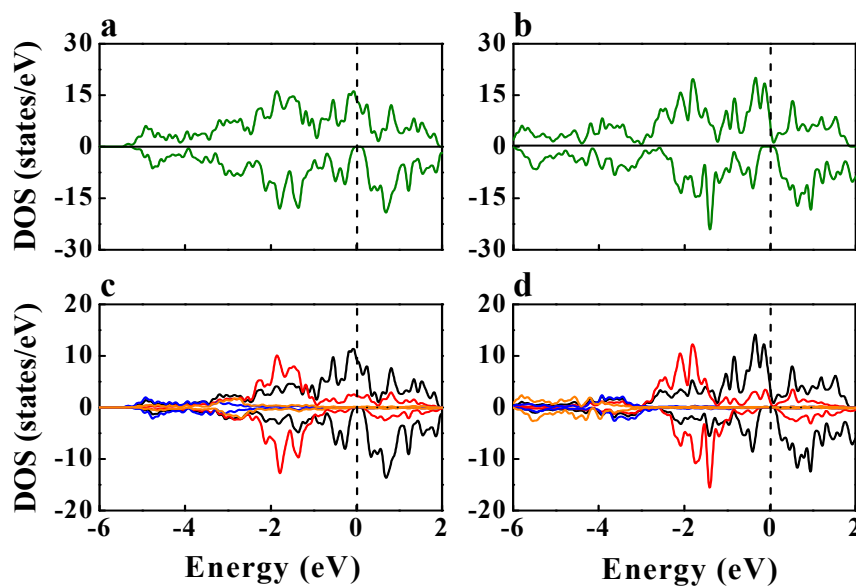


Figure 7. The total density of the states (DOS) of (a) $\text{Ti}_{2.25}\text{Co}_{0.75}\text{Si}_{0.5}\text{B}_{0.5}$ and (b) $\text{Ti}_{2.25}\text{Co}_{0.75}\text{Si}_{0.5}\text{P}_{0.5}$ at the equilibrium lattice parameters. The partial DOS of (c) $\text{Ti}_{2.25}\text{Co}_{0.75}\text{Si}_{0.5}\text{B}_{0.5}$ and (d) $\text{Ti}_{2.25}\text{Co}_{0.75}\text{Si}_{0.5}\text{P}_{0.5}$ at the equilibrium lattice parameters. The black, red, blue, and orange solid lines indicate the Ti-d, Co-d, Si-p, and B (P)-p states, respectively.

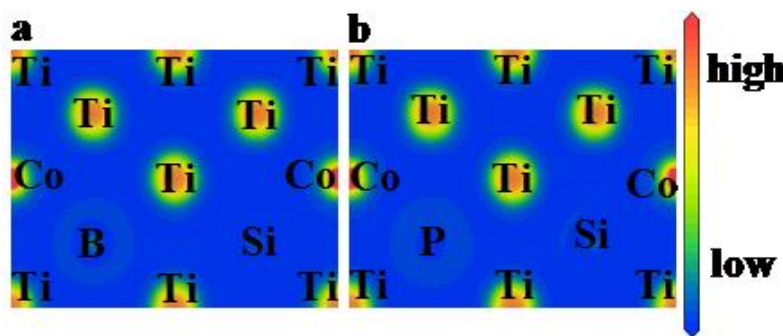


Figure 8. The spin densities of (a) $\text{Ti}_{2.25}\text{Co}_{0.75}\text{Si}_{0.5}\text{B}_{0.5}$ and (b) $\text{Ti}_{2.25}\text{Co}_{0.75}\text{Si}_{0.5}\text{P}_{0.5}$ at the equilibrium lattice parameters.

4. Conclusions

In summary, we have determined the structural, electronic, and magnetic properties of inverse Ti_2CoSi -based compounds. By adjusting the concentration of titanium and cobalt, the fabricated $\text{Ti}_{2.25}\text{Co}_{0.75}\text{Si}$ compound is half metallic, that is, single-channel spin polarized. The majority-spin bands are strongly metallic, while the minority-spin bands are semiconductor-like around the Fermi level. This gap has previously been reported by other authors, and is formed as a result of the strong 3d–3d hybridization between the two transition-metal atoms [42–45]. It is thought that this 3d–3d interaction is essential for the formation of the gap at the Fermi level. Under the influence of isotropic hydrostatic pressure, the $\text{Ti}_{2.25}\text{Co}_{0.75}\text{Si}$ alloy can preserve the half-metallic feature between a range of 5.78 Å to 6.35 Å. Nevertheless, it would transform to a gapless half metal upon the tetragonalization of the lattice. Tetragonal deformation could modify the crystal symmetry and vary the position of the edge of the bands, especially at some high-symmetry points in the reciprocal space. Our further calculations on $\text{Ti}_{2.25}\text{Co}_{0.75}\text{Si}_{0.5}\text{B}_{0.5}$, $\text{Ti}_{2.25}\text{Co}_{0.75}\text{Si}_{0.5}\text{P}_{0.5}$, and other doped compounds demonstrate that the doped foreign impurity is able to adjust the valence electron concentration of the compound and shift the Fermi level upwards or downwards, creating several different electronic structures around the sensitive Fermi level.

Author Contributions: S.D. and L.F. designed the project. L.Z. and J.D. performed the calculations and prepared the manuscript. All of the authors analyzed the data and discussed the results. All authors have read and agreed to the published version of the manuscript.

Funding: This research was funded by the National Natural Science Foundation of China (grant no's. 61804010, 11204209, 60876035, and 61874004), the Natural Science Foundation of Tianjin City (grant no. 17JCYBJC16200), and the Project of Guangdong Baiyun University (grant no. 2017BYKY29).

Conflicts of Interest: The authors declare no conflict of interest.

References

1. Brown, P.J.; Neumann, K.U.; Webster, P.J.; Ziebeck, K.R.A. The magnetization distributions in some Heusler alloys proposed as half-metallic ferromagnets. *J. Phys. Condens. Matter* **2000**, *12*, 1827. [[CrossRef](#)]
2. Žutić, I.; Fabian, J.; Sarma, S.D. Spintronics: Fundamentals and applications. *Rev. Mod. Phys.* **2004**, *76*, 323. [[CrossRef](#)]
3. Berri, S. First-Principles Calculations to Investigate the Structural, electronic, and half-metallic properties of $Ti_2RhSn_{1-x}Si_x$, $Ti_2RhSn_{1-x}Ge_x$, and $Ti_2RhGe_{1-x}Si_x$ ($x = 0, 0.25, 0.5, 0.75$, and 1) quaternary Heusler alloys. *J. Supercond. Nov. Magn.* **2019**, *32*, 2219–2228. [[CrossRef](#)]
4. Alijani, V.; Winterlik, J.; Fecher, G.H.; Naghavi, S.S.; Felser, C. Quaternary half-metallic Heusler ferromagnets for spintronics applications. *Phys. Rev.* **2011**, *83*, 184428. [[CrossRef](#)]
5. Gao, G.Y.; Hu, L.; Yao, K.L.; Luo, B.; Liu, N. Large half-metallic gaps in the quaternary Heusler alloys $CoFeCrZ$ ($Z = Al, Si, Ga, Ge$): A first-principles study. *J. Alloy Compd.* **2013**, *551*, 539–543. [[CrossRef](#)]
6. Singh, M.; Saini, H.S.; Thakur, J.; Reshak, A.H.; Kashyap, M.K. Electronic structure, magnetism and robust half-metallicity of new quaternary Heusler alloy $FeCrMnSb$. *J. Alloy Compd.* **2013**, *580*, 201–204. [[CrossRef](#)]
7. Özdoğan, K.; Şaşıoğlu, E.; Galanakis, I. Slater-Pauling behavior in $LiMgPdSn$ -type multifunctional quaternary Heusler materials: Half-metallicity, spin-gapless and magnetic semiconductors. *J. Appl. Phys.* **2013**, *113*, 193903. [[CrossRef](#)]
8. Zhang, Y.J.; Liu, Z.H.; Li, G.T.; Ma, X.Q.; Liu, G.D. Magnetism, band gap and stability of half-metallic property for the quaternary Heusler alloys $CoFeTiZ$ ($Z = Si, Ge, Sn$). *J. Alloy Compd.* **2014**, *616*, 449–453. [[CrossRef](#)]
9. Xiong, L.; Yi, L.; Gao, G.Y. Search for half-metallic magnets with large half-metallic gaps in the quaternary Heusler alloys $CoFeTiZ$ and $CoFeVZ$ ($Z = Al, Ga, Si, Ge, As, Sb$). *J. Magn. Magn. Mater.* **2014**, *360*, 98–103. [[CrossRef](#)]
10. Al-zyadi, J.M.K.; Gao, G.Y.; Yao, K.L. Theoretical investigation of the electronic structures and magnetic properties of the bulk and surface (001) of the quaternary Heusler alloy $NiCoMnGa$. *J. Magn. Magn. Mater.* **2015**, *378*, 1–6. [[CrossRef](#)]
11. Felser, C.; Wollmann, L.; Chadov, S.; Fecher, G.H.; Parkin, S.S. Basics and prospective of magnetic Heusler compounds. *APL Mater.* **2015**, *3*, 041518. [[CrossRef](#)]
12. Kundu, A.; Ghosh, S.; Banerjee, R.; Ghosh, S.; Sanyal, B. New quaternary half-metallic ferromagnets with large Curie temperatures. *Sci. Rep.* **2017**, *7*, 1803. [[CrossRef](#)] [[PubMed](#)]
13. Wang, X.L. Proposal for a new class of materials: Spin gapless semiconductors. *Phys. Rev. Lett.* **2008**, *100*, 156404. [[CrossRef](#)] [[PubMed](#)]
14. Ouardi, S.; Fecher, G.H.; Felser, C.; Kubler, J. Realization of spin gapless semiconductors: The Heusler compound Mn_2CoAl . *Phys. Rev. Lett.* **2013**, *110*, 100401. [[CrossRef](#)]
15. Heusler, F. Über magnetische manganlegierungen. *Verh. Dtsch. Phys. Ges.* **1903**, *5*, 219.
16. Jiang, D.G.; Ye, Y.X.; Yao, W.B.; Zeng, D.W.; Zhou, J.; Liu, L.N.; Wen, Y.F. First-principles calculations of the structural, magnetic, and electronic properties of Fe_2MgB full-Heusler alloy. *J. Electron. Mater.* **2019**, *48*, 7258–7262. [[CrossRef](#)]
17. Moodera, J.S.; Nassar, J.; Mathon, G. Spin-tunneling in ferromagnetic junctions. *Annu. Rev. Mater.* **1999**, *29*, 381. [[CrossRef](#)]
18. Skaftouros, S.; Ozdogan, K.; Sasioglu, E.; Galanakis, I. Search for spin gapless semiconductors: The case of inverse Heusler compounds. *Appl. Phys. Lett.* **2013**, *102*, 022402. [[CrossRef](#)]
19. Xu, G.Z.; Liu, E.K.; Du, Y.; Li, G.J.; Liu, G.D.; Wang, W.H.; Wu, G.H. A new spin gapless semiconductors family: Quaternary Heusler compounds. *Europhys. Lett.* **2013**, *102*, 17007. [[CrossRef](#)]

20. Kudryavtsev, Y.V.; Oksenenko, V.A.; Lee, Y.P.; Hyun, Y.H.; Kim, J.B.; Park, J.S.; Park, S.Y.; Dubowik, J. Evolution of the magnetic properties of Co₂MnGa Heusler alloy films: From amorphous to ordered films. *Phys. Rev. B* **2007**, *76*, 024430. [[CrossRef](#)]
21. Jamer, M.E.; Assaf, B.A.; Devakul, T.; Heiman, D. Magnetic and transport properties of Mn₂CoAl oriented films. *Appl. Phys. Lett.* **2013**, *103*, 142403. [[CrossRef](#)]
22. Xu, G.Z.; Du, Y.; Zhang, X.M.; Zhang, H.G.; Liu, E.K.; Wang, W.H.; Wu, G.H. Magneto-transport properties of oriented Mn₂CoAl films sputtered on thermally oxidized Si substrates. *Appl. Phys. Lett.* **2014**, *104*, 242408. [[CrossRef](#)]
23. Feng, W.W.; Fu, X.; Wan, C.H.; Yuan, Z.H.; Han, X.F.; Quang, N.V.; Cho, S. Spin gapless semiconductor like Ti₂MnAl film as a new candidate for spintronics application. *Phys. Status Solidi RRL* **2015**, *9*, 641. [[CrossRef](#)]
24. Lukashev, P.; Kharel, P.; Gilbert, S.; Staten, B.; Hurley, N.; Fuglsby, R.; Huh, Y.; Valloppilly, S.; Zhang, W.; Yang, K.; et al. Investigation of spin-gapless semiconductivity and half-metallicity in Ti₂MnAl-based compounds. *Appl. Phys. Lett.* **2016**, *108*, 141901. [[CrossRef](#)]
25. Dulal, R.P.; Dahal, B.R.; Forbes, A.; Bhattarai, N.; Pegg, I.L.; Philip, J. Weak localization and small anomalous Hall conductivity in ferromagnetic Weyl semimetal Co₂TiGe. *Sci. Rep.* **2019**, *9*, 3342. [[CrossRef](#)] [[PubMed](#)]
26. Dahal, B.; Huber, C.; Zhang, W.; Valloppilly, S.; Huh, Y.; Kharel, P.; Sellmyer, D. Effect of partial substitution of In with Mn on the structural, magnetic, and magnetocaloric properties of Ni₂Mn_{1+x}In_{1-x} Heusler alloys. *J. Phys. D Appl. Phys.* **2019**, *52*, 425305. [[CrossRef](#)]
27. Casper, F.; Graf, T.; Chadov, S.; Balke, B.; Felser, C. Half-Heusler compounds: Novel materials for energy and spintronic applications. *Semicond. Sci. Technol.* **2012**, *27*, 063001. [[CrossRef](#)]
28. Graf, T.; Felser, C.; Parkin, S.S.P. Simple rules for the understanding of Heusler compounds. *Prog. Solid State Chem.* **2011**, *39*, 1–50. [[CrossRef](#)]
29. Kandpal, H.C.; Fecher, G.H.; Felser, C. Calculated electronic and magnetic properties of the half-metallic, transition metal based Heusler compounds. *J. Phys. D Appl. Phys.* **2007**, *40*, 1507. [[CrossRef](#)]
30. Bradley, A.J.; Rodgers, J.W. The crystal structure of the Heusler alloys. *Proc. R. Soc. Lond. Ser. A* **1934**, *144*, 340. [[CrossRef](#)]
31. Payne, M.C.; Teter, M.P.; Allan, D.C.; Arias, T.A.; Joannopoulos, J.D. Iterative minimization techniques for *ab initio* total-energy calculations: Molecular dynamics and conjugate gradients. *Rev. Mod. Phys.* **1992**, *64*, 1065. [[CrossRef](#)]
32. Vanderbilt, D. Soft self-consistent pseudopotentials in a generalized eigenvalue formalism. *Phys. Rev. B* **1990**, *41*, 7892. [[CrossRef](#)] [[PubMed](#)]
33. Milman, V.; Winkler, B.; White, J.A.; Pickard, C.J.; Payne, M.C.; Akhmatkaya, E.V.; Nobes, R.H. Electronic structure, properties, and phase stability of inorganic crystals: A pseudopotential plane-wave study. *Int. J. Quantum Chem.* **2000**, *77*, 895. [[CrossRef](#)]
34. Segall, M.D.; Lindan, P.J.D.; Probert, M.J.; Pickard, C.J.; Hasnip, P.J.; Clark, S.J.; Payne, M.C. First-principles simulation: Ideas, illustrations and the CASTEP code. *J. Phys. Condens. Matter* **2002**, *14*, 2717. [[CrossRef](#)]
35. Clark, S.J.; Segall, M.D.; Pickard, C.J.; Hasnip, P.J.; Probert, M.I.J.; Refson, K.; Payne, M.C. First principles methods using CASTEP. *Z. Krist. Cryst. Mater.* **2005**, *220*, 567–570. [[CrossRef](#)]
36. Hasnip, P.J.; Refson, K.; Probert, M.I.J.; Yates, J.R.; Clark, S.J.; Pickard, C.J. Density functional theory in the solid state. *Philos. Trans. R. Soc. A* **2014**, *372*, 20130270. [[CrossRef](#)]
37. Perdew, J.P.; Chevary, J.A.; Vosko, S.H.; Jackson, A.; Pederson, M.R.; Fiolhais, C. Atoms, molecules, solids, and surfaces: Applications of the generalized gradient approximation for exchange and correlation. *Phys. Rev. B* **1992**, *46*, 6671. [[CrossRef](#)] [[PubMed](#)]
38. Perdew, J.P.; Burke, K.; Ernzerhof, M. Generalized gradient approximation made simple. *Phys. Rev. Lett.* **1996**, *77*, 3865. [[CrossRef](#)] [[PubMed](#)]
39. Waybright, J.; Halbritter, L.; Dahal, B.; Qian, H.; Huh, Y.; Lukashev, P.; Kharel, P. Structure and magnetism of NiFeMnGa_xSn_{1-x} (x = 0, 0.25, 0.5, 0.75, 1.00) Heusler compounds. *AIP Adv.* **2019**, *9*, 035105. [[CrossRef](#)]
40. Wu, B.; Huang, H.; Zhou, G.; Feng, Y.; Chen, Y.; Wang, X. Structure, magnetism, and electronic properties of inverse Heusler alloy Ti₂CoAl/MgO(100) heterojunction: The role of interfaces. *Appl. Sci.* **2018**, *8*, 2336. [[CrossRef](#)]
41. Wu, B.; Huang, H.; Li, P.; Zhou, T.; Zhou, G.; Feng, Y.; Chen, Y. First-principles study on the structure, magnetism, and electronic properties in inverse Heusler alloy Ti₂FeAl/GaAs(100) heterojunction. *Superlatt. Microstruct.* **2019**, *133*, 106205. [[CrossRef](#)]

42. Fujii, S.; Ishida, S.; Asano, S. A half-metallic band structure and Fe_2MnZ ($Z = \text{Al, Si, P}$). *J. Phys. Soc. Jpn.* **1995**, *64*, 185–191. [[CrossRef](#)]
43. Ishida, S.; Fujii, S.; Kashiwagi, S.; Asano, S. Search for half-metallic compounds in Co_2MnZ ($Z = \text{III}^b, \text{IV}^b, \text{V}^b$ element). *J. Phys. Soc. Jpn.* **1995**, *64*, 2152–2157. [[CrossRef](#)]
44. Miura, Y.; Shirai, M.; Nagao, K. Ab initio study on stability of half-metallic Co-based full-Heusler alloys. *J. Appl. Phys.* **2006**, *99*, 08J112. [[CrossRef](#)]
45. Mebsout, R.; Amari, S.; Méçabih, S.; Abbar, B.; Bouhafs, B. Spin-Polarized Calculations of Magnetic and Thermodynamic Properties of the Full-Heusler MnZ ($Z = \text{Al, Ga}$). *Int. J. Thermophys.* **2013**, *34*, 507–520. [[CrossRef](#)]



© 2020 by the authors. Licensee MDPI, Basel, Switzerland. This article is an open access article distributed under the terms and conditions of the Creative Commons Attribution (CC BY) license (<http://creativecommons.org/licenses/by/4.0/>).